Environmental Pollution 228 (2017) 92–101

Contents lists available at ScienceDirect

Environmental Pollution

journal homepage: www.elsevier.com/locate/envpol

Source characterization of urban particles from meat smoking activities in Chongqing, China using single particle aerosol mass spectrometry

Yang Chen [a, c, *], John C. Wenger [b], Fumo Yang [a, d, e, **], Junji Cao [c], Rujin Huang [c], Guangming Shi [a], Shumin Zhang [f, g], Mi Tian [a], Huanbo Wang [a]

[a] Research Center for Atmospheric Environment, Chongqing Institute of Green and Intelligent Technology, Chinese Academy of Sciences, Chongqing 400714, China
[b] Department of Chemistry and Environmental Research Institute, University College Cork, Cork, Ireland
[c] Key Lab of Aerosol Chemistry & Physics, Institute of Earth Environment, Chinese Academy of Sciences, Xi'an 710061, China
[d] Center for Excellence in Regional Atmospheric Environment, Institute of Urban Environment, Chinese Academy of Sciences, Xiamen 361021, China
[e] Yangtze Normal University, Chongqing 408100, China
[f] North Sichuan Medical College, Nanchong 637000, Sichuan, China
[g] Chongqing University, Chongqing 400044, China

ARTICLE INFO

Article history:
Received 14 December 2016
Received in revised form
4 May 2017
Accepted 7 May 2017

Keywords:
Biomass burning
Meat smoking
Chongqing
SPAMS
$PM_{2.5}$
Biofuel smoldering

ABSTRACT

A Single Particle Aerosol Mass Spectrometer (SPAMS) was deployed in the urban area of Chongqing to characterize the particles present during a severe particulate pollution event that occurred in winter 2014–2015. The measurements were made at a time when residents engaged in traditional outdoor meat smoking activities to preserve meat before the Chinese Spring Festival. The measurement period was predominantly characterized by stagnant weather conditions, highly elevated levels of $PM_{2.5}$, and low visibility. Eleven major single particle types were identified, with over 92.5% of the particles attributed to biomass burning emissions. Most of the particle types showed appreciable signs of aging in the stagnant air conditions. To simulate the meat smoking activities, a series of controlled smoldering experiments was conducted using freshly cut pine and cypress branches, both with and without wood logs. SPAMS data obtained from these experiments revealed a number of biomass burning particle types, including an elemental and organic carbon (ECOC) type that proved to be the most suitable marker for meat smoking activities. The traditional activity of making preserved meat in southwestern China is shown here to be a major source of particulate pollution. Improved measures to reduce emissions from the smoking of meat should be introduced to improve air quality in regions where smoking meat activity prevails.

1. Introduction

Biomass burning (BB) emissions make a significant contribution to urban PM in China (Cao et al., 2007; Cheng et al., 2014; He et al., 2011; Huang et al., 2014; Yang et al., 2011). A range of BB activities has been identified, including forest and savanna wildfires, wood and peat burning, residential heating and cooking, as well as industrial biofuel burning (Reid et al., 2005; Simoneit, 2002). Zhang and Cao (2015) have highlighted two of the most important BB sources in China: household biofuel combustion and open agricultural waste burning in rural areas. BB particles impact considerably on urban air quality in China during periods of agricultural waste burning. For example, it has been estimated that $PM_{2.5}$ levels for the Yangtze River Delta region could be reduced by 51% if anthropogenic biomass burning is eliminated (Cheng et al., 2014). Detailed investigation of chemical composition and mixing state of atmospheric single particles can provide information on their sources, as well as the extent of aging or atmospheric processing.

* Corresponding author. Research Center for Atmospheric Environment, Chongqing Institute of Green and Intelligent Technology, Chinese Academy of Sciences, Chongqing 400714. China.
** Corresponding author. Research Center for Atmospheric Environment, Chongqing Institute of Green and Intelligent Technology, Chinese Academy of Sciences, Chongqing 400714. China.
E-mail addresses: chenyang@cigit.ac.cn (Y. Chen), fmyang@cigit.ac.cn (F. Yang).

http://dx.doi.org/10.1016/j.envpol.2017.05.022
0269-7491/

Over the last 15 years, single particle mass spectrometers have been used for determining the size-resolved chemical characterization of individual BB particles for source identification and apportionment (Pratt and Prather, 2012). Silva et al. (1999) investigated the composition and mixing state of typical wood-burning particles in southern California, while Healy et al. (2010) reported the chemical composition of freshly emitted particles from wood and peat burning in Cork, Ireland and used the data to identify the sources of ambient particles. Pratt et al. (2011) characterized the aging of BB particles in two prescribed burn smoke plumes using an aircraft-based instrument, and Pagels et al. (2013) investigated various markers of solid biofuel combustion particles. Overall, the available literature in this area indicates that BB particles are typically rich in potassium, Elemental Carbon (EC), and Organic Carbon (OC), with the latter comprised of numerous combustion products including levoglucosan, aldehydes, ketones, polycyclic aromatic hydrocarbons (PAHs), and nitrogenated organics. Aged or processed BB particles usually contain significant amounts of secondary nitrate and sulfate (Pagels et al., 2013; Pratt et al., 2011; Zauscher et al., 2013). Over the last few years, single particle aerosol mass spectrometers (SPAMS) have been used to study the size-resolved chemical characterization and mixing state of ambient PM at various locations in China. Ambient BB particle types have been reported in Guangzhou (Bi et al., 2011), Nanjing (Wang et al., 2015), Shanghai (Huang et al., 2013), Beijing (Li et al., 2014), Xi'an (Chen et al., 2016), and Mt. Huang (Chen et al., 2014). However, the characterization of single particles in urban areas of southwestern China is still limited (Chen et al., 2017).

Chongqing is a municipality in the southwestern China, with a population of 8.23 million in the main city (Chen et al., 2017). In both the urban and rural areas of Chongqing, natural gas is commonly used for residential cooking, but biofuel is still widely used in traditional restaurants and for smoking meat usually one or two months before the Chinese Spring Festival (January or February). These meat smoking activities are usually performed outdoors in areas close to residential communities, and the resulting emissions have attracted significant attention from the scientific community to general public within the wider context of particulate pollution in China. However, information on the impacts of traditional meat smoking activities on local and regional air quality is still limited and further targeted scientific studies are needed.

The aim of this study was to investigate the single particle chemical composition of ambient particles using a SPAMS in Chongqing during the traditional meat-smoking period. Measurements were made during a severe particulate pollution event that occurred in Chongqing from 25th December 2014 to 8th January 2015. Detailed analysis of the SPAMS dataset showed that the single particle population was dominated by BB types and the contribution of meat smoking was confirmed by the presence of particle types also observed in a series of controlled biomass smoldering experiments. This study thus provides a unique insight into the sources, composition, and mixing state of BB particles produced from meat smoking activities and their impact on air quality in the urban area of Chongqing. The findings are also relevant for other urban areas of China where meat smoking activities are common in winter.

2. Methods

2.1. Field measurements

The sampling site is an air quality monitoring station established in 2010 to monitor the urban air quality of Chongqing (Fig. 1). A detailed description of the sampling site is available in the literature (Chen et al., 2017). It is located on the roof of a building, 30 m above the ground (106.51°E, 29.62°N), in a typical commercial and residential area, 10 km from the city center. A range of gaseous air pollutants, including nitrogen oxides (NOx), ozone, carbon monoxide, and SO_2 is routinely monitored at this urban background site. $PM_{2.5}$ mass concentration is measured continuously using a Tapered Element Oscillating Microbalance (TEOM, 1400a, Thermo Fisher, USA). The mass concentration of Black Carbon was measured using an Aethalometer (AE33, Magee, USA) and meteorological data were collected using a weather station (Vaisala MAWS201, Finland).

In this study, a Single Particle Aerosol Mass Spectrometer (SPAMS, HeXin, China) was also deployed at the site to measure the size-resolved chemical composition of single particles during a sustained air pollution event that occurred in late December 2014 and early January 2015. A technical description of the SPAMS was provided by Li et al. (2011a). Briefly, the sampled air passes through an aerodynamic lens which transmits particles with aerodynamic diameters in the range 0.1–2.0 μm with high efficiency. The resulting particle beam is directed towards a sizing region where the vacuum aerodynamic diameter (D_{va}) is determined by the time-of-flight between two pre-positioned laser beams (Nd:YAG, 532 nm). Particles subsequently enter the mass spectrometer region and are ionized using a Nd:YAG laser operating at a wavelength of 266 nm (~1 mJ/pulse, 1×10^8 W/cm^2, UL728F11-F115, Quantel, France). The resulting positive and negative ions are analyzed in two time-of-flight mass spectrometers, yielding a positive and a negative ion mass spectrum for each single particle. The SPAMS thus provides information on the chemical composition and mixing state of single particles. It should be noted that this instrument is different from the Aerodyne Soot Particle Aerosol Mass Spectrometer (SP-AMS), which is used to measure the size, mass and chemical composition of black carbon containing particles (Onasch et al., 2012; Wang et al., 2016).

Air mass backward trajectories were calculated using the Hybrid Single Particle Lagrangian Integrated Trajectory (HYSPLIT) model to elucidate the origin of air masses during the pollution event (Draxler and Hess, 1998). All the trajectory calculations were performed using a height of 500 m above ground level (AGL) at 00:00 local time using GDAS1 meteorological dataset.

2.2. Controlled smoldering experiments

A number of controlled smoldering experiments were performed to simulate the emissions arising from the meat smoking activities. The traditional approach typically involves the smoldering of freshly cut pine and cypress branches (with green needles) along with dry wood for 12–48 h to smoke the meat. The oxygen supply is controlled to avoid flaming. The experiments performed here mimicked this process in a homemade oven using locally available wood combined with fresh pine and cypress branches, with the latter making up less than 30% (by weight) of the total biomass in the smoking procedure. Another set of smoldering experiments was conducted using only the fresh pine and cypress branches in order to exclude the influence of BB particles from the combustion of dry wood. The SPAMS instrument was used to sample the emissions continuously in order to obtain representative single particle mass spectra of the biomass smoke that would serve as potential markers to aid interpretation of the field data. The inlet of the SPAMS was fitted with a cyclone impactor to remove particles with a diameter >2.5 μm. Neither dilution nor relative humidity control was adopted during the SPAMS sampling.

2.3. SPAMS data analysis

A total of 1.24 million ambient particles were collected with

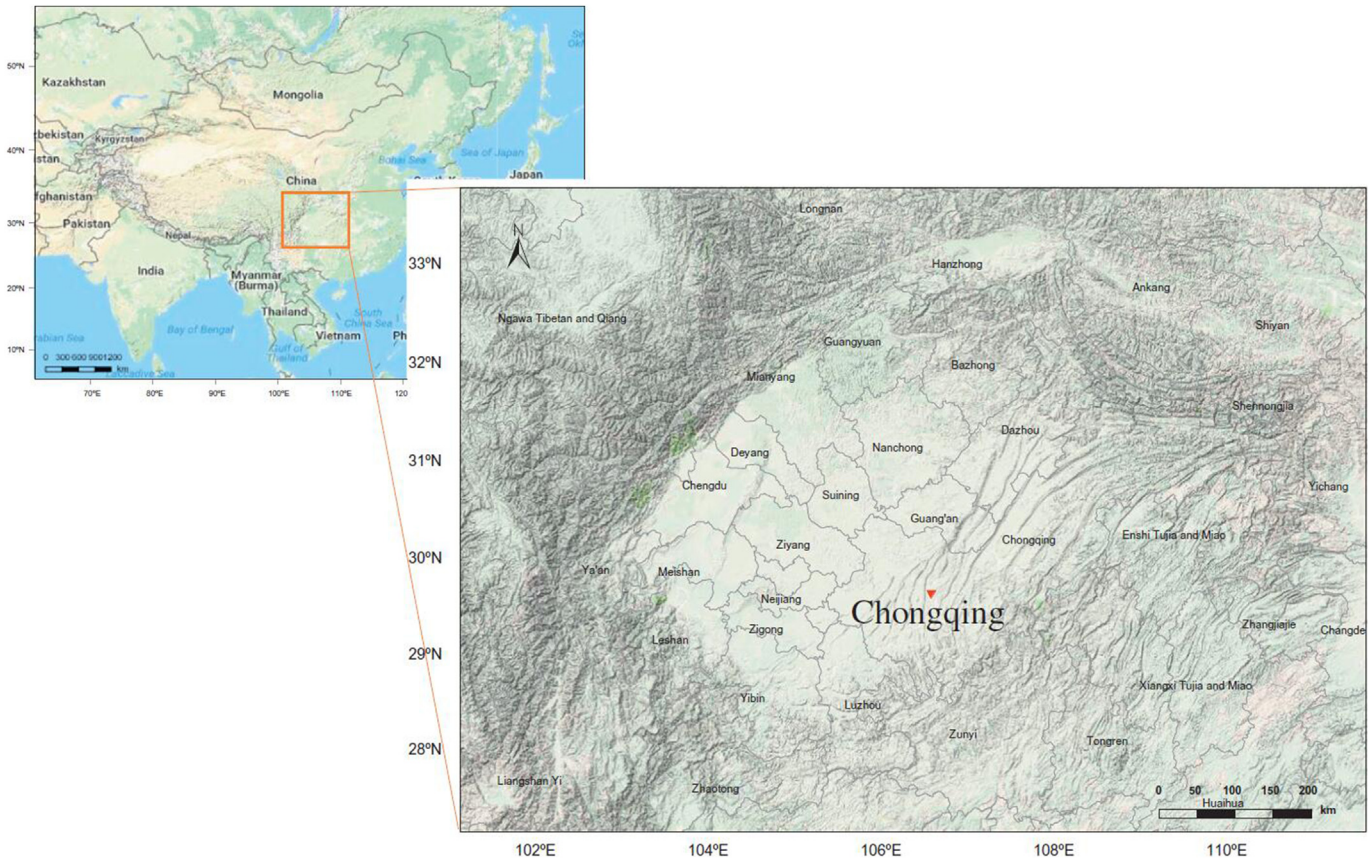

Fig. 1. Sampling site in Chongqing.

validated mass spectra (30 units above the baseline) from 25th December 2014 to 8th January 2015. The SPAMS data were imported into the YAADA toolkit (Software Toolkit to Analyze Single-Particle Mass Spectral Data, v 2.11) which was embedded in MATLAB (2012b). An adaptive resonance theory based neural network algorithm (ART-2a) clustering procedure (Song et al., 1999) was applied with a vigilance factor of 0.80, a learning rate of 0.05, and 20 iterations. These vigilance factors have been commonly used in previous studies (Cao, 2014; Yang et al., 2012). This procedure produced 236 particle clusters, many of which exhibited similar mass spectra with small differences in ion peak areas. A well-established strategy based on similar temporal trend, mass spectra and size distribution was adopted to manually merge the particle types into 11 distinct groups (Dall'osto and Harrison, 2006).

SPAMS data collected during the controlled smoldering experiments were also analyzed using the procedures outlined above. The same ART-2a parameter settings were applied to cluster the particles and to separate the biomass burning particle types produced during the smoldering process from those observed as background particles in the ambient air (mostly aged BB and EC particle types).

3. Results and discussion

3.1. Pollution event overview

The average values for various meteorological parameters, $PM_{2.5}$, BC, and gasses measured during the measurement campaign are summarized in Table 1. The hourly SPAMS count was well correlated to $PM_{2.5}$ mass concentration ($R = 0.64$). The temporal variation of the data collected during the campaign is shown in Fig. 2. Based on the changes in single particle composition, the data can be separated into three stages. Stage I, from 12/25/2014 to 12/26/2015, was before the sustained pollution event, which is labeled Stage II and occurred from 12/26/2014 to 01/06/2015. During Stage II, the stagnant air conditions significantly restricted dispersion of local pollutants and resulted in high $PM_{2.5}$ mass (Fig. 2a) and poor visual range (Fig. 2c). The $PM_{2.5}$ concentration reached its highest value at 238 μg m^{-3} on 01/04/2015 in response, the local government issued an immediate ban on wood burning, which in principle, included meat smoking activities and biofuel use in restaurants for cooking purposes. After the ban, the $PM_{2.5}$ and BC mass concentrations initially showed a significant decrease (Fig. 2a), which may also be due partly to a period of rainfall. However, the $PM_{2.5}$ concentration increased to 200 μg m^{-3} during daylight hours on 01/05/2015 and the visual range returned to below 3 km. Another period of rain, combined with increased wind speeds late on 01/05/2015 caused pollutant levels to drop quickly and sustained winds on 01/06/2015 led to the end of the pollution event as $PM_{2.5}$ levels fell to around 50 μg m^{-3}, Stage III.

3.2. Single particle types

Eleven clusters were resolved and named according to source type or the dominant ions present in the average mass spectra (Fig. 3). Some of these particle types have been reported in the literature (Bi et al., 2011; Chen et al., 2017; Dall'osto and Harrison, 2006; Healy et al., 2010; Pratt and Prather, 2012; Qin et al., 2012).

BB (33.0% in number fraction). The positive mass spectrum shows a strong signal for potassium (m/z 39, m/z 41) as well as

Table 1
Summary of meteorological parameters, particulate, and gaseous pollutants during the measurement campaign.

Meteorological parameter		Average	Stage I	Stage II	Stage III
Wind Speed	($m\ s^{-1}$)	1.0 ± 0.40	0.9 ± 0.2	0.8 ± 0.2	1.5 ± 0.6
RH	(%)	75.6 ± 6.6	77.8 ± 8.3	76.0 ± 9.6	75.0 ± 5.3
Visual Range	(km)	2.2 ± 0.6	1.8 ± 0.3	2.2 ± 0.6	4.6 ± 1.6
Temperature	(°C)	8.4 ± 1.4	8.2 ± 1.5	8.5 ± 2.2	8.5 ± 2.0
PM					
($\mu g\ m^{-3}$)	BC	9.1 ± 2.8	10.1 ± 3.6	8.2 ± 2.1	4.8 ± 0.8
	$PM_{2.5}$	155 ± 39	181 ± 47	148 ± 22	72 ± 13
Gasses					
(ppb)	NO	123 ± 49	140 ± 32	135 ± 23	73 ± 15
	NO_2	41 ± 8	35 ± 4	46 ± 12	26 ± 7
	O_3	6 ± 3	10 ± 5	5 ± 2	6 ± 3
	CO	458 ± 213	693 ± 188	413 ± 105	312 ± 81
	SO_2	9 ± 5	11 ± 4	9 ± 4	5 ± 2

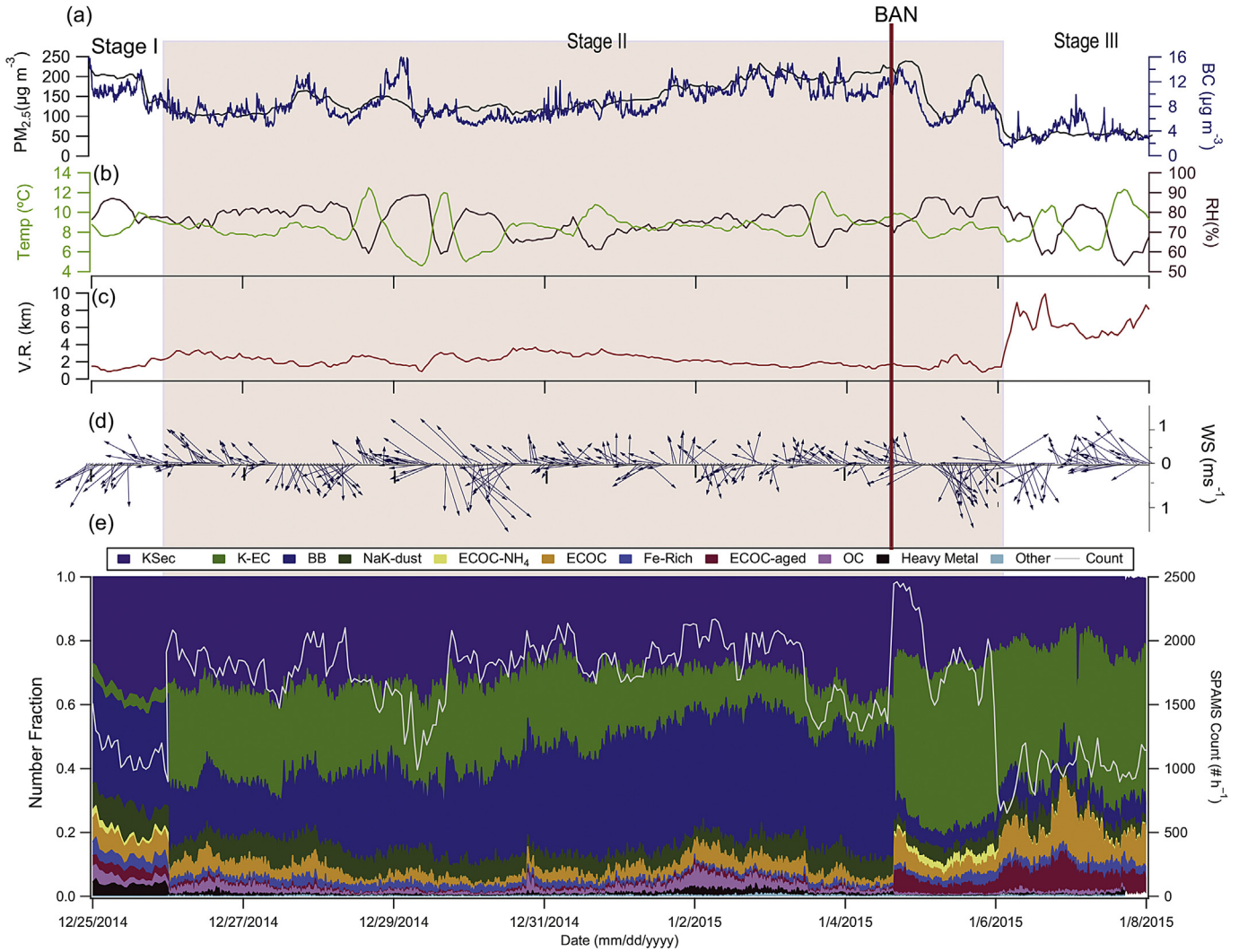

Fig. 2. Time series of (a) $PM_{2.5}$ (left) and BC (right); (b) Temperature (left), RH (right); (c) Visual Range (V.R.); (d) Wind speed and wind direction (North is parallel with Y axis); (e) SPAMS ART-2a cluster number fraction and counts per hour.

peaks due to $[K_2Cl]^+$ (m/z 113, m/z 115) and EC (m/z 12, 24, 36, 48). In the negative spectrum, EC, $[CN]^-$ (m/z −26) and $[CNO]^-$ (m/z −42) are typical markers of BB particles (Silva et al., 1999). $[CHO_2]^-$ (m/z −45), $[C_2H_3O_2]^-$ (m/z −59) and $[C_3H_3O_2]^-$ (m/z −71) were also observed as fragments of levoglucosan (Silva et al., 1999), along with peaks due to nitrate (m/z −46 and −62) and sulfate (m/z −80 and −97).

K-EC (20.0%). Potassium and carbon fragments (C_n^+ and C_n^-) are

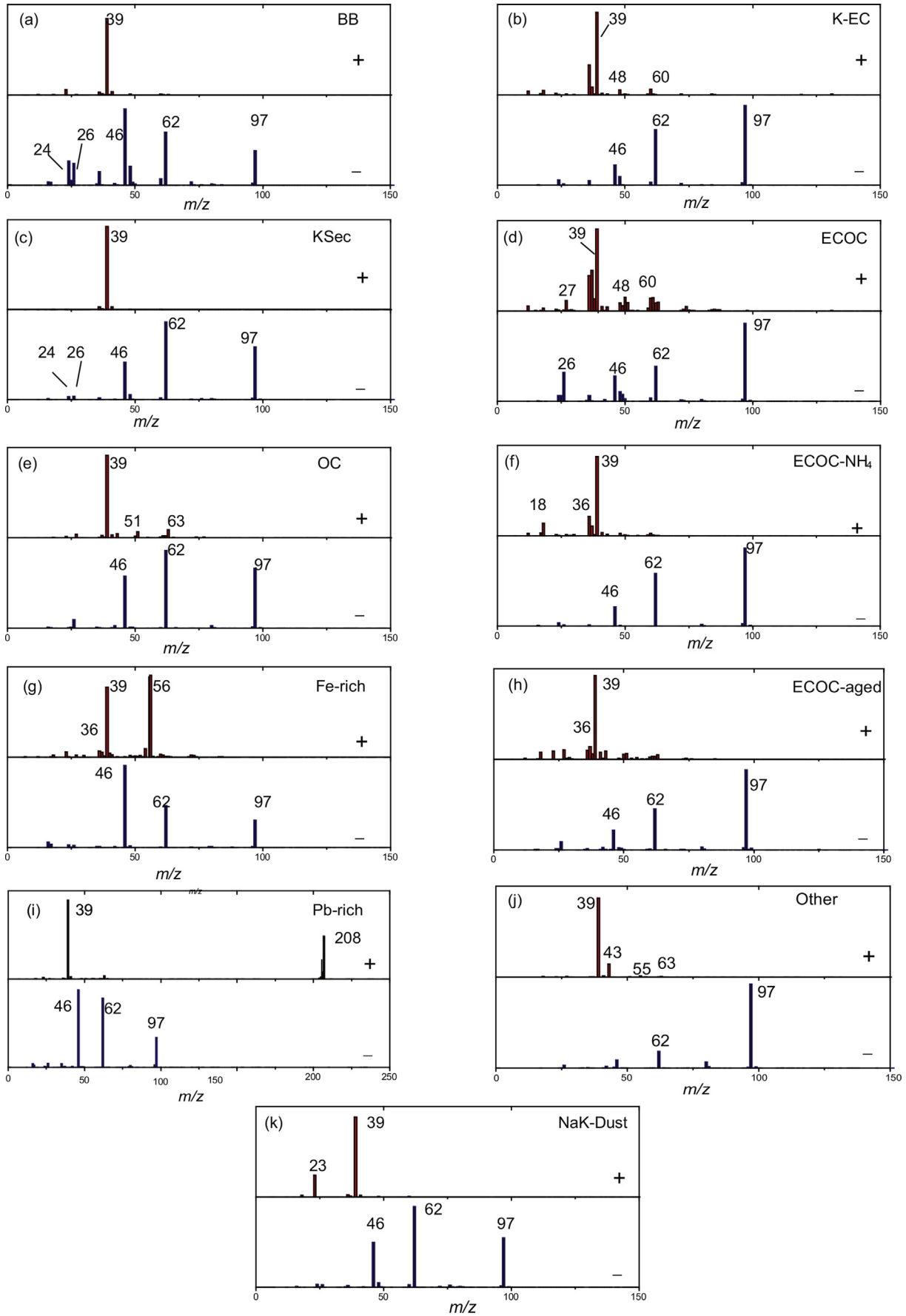

Fig. 3. Average mass spectra of the eleven ART-2a clusters: (a) Biomass burning (BB); (b)Potassium-rich Elemental Carbon (K-EC); (c) K-Secondary (KSec); (d) Internally mixed EC-OC (ECOC); (e) OC; (f) ECOC-NH_4; (g) Fe-rich; (h) ECOC-aged; (i) Pb-rich; (j) Other; (k) Sodium and Potassium rich dust (NaK-dust).

pronounced in the average mass spectrum for this particle type, which has been identified as a biomass burning particle type in previous studies (Healy et al., 2012; Huang et al., 2013; Zhang et al., 2015).

KSec (29.0%). The average mass spectrum for this particle type is similar to that of BB, except that the organic ions (e.g. $[CH_3CO]^+$, $[C_2H_3]^+$, $[C_3H_7]^+$, and $[C_6H_5]^+$, etc.) in the average positive mass spectrum are weaker, while the sulfate and nitrate signals in the negative spectrum are stronger. This suggests that the particles are aged BB particles that have undergone a significant amount of processing, such as removal of semi-volatile species (Jimenez et al., 2009; Robinson et al., 2007), formation of organic acids, and uptake of inorganic species after being emitted from plume (Pratt et al., 2011). These aged K-rich particles from biomass burning were typically spherical in morphology due to secondary species coating (Li et al., 2010; Pratt et al., 2010).

ECOC (5.0%). Potassium and carbon are dominant in the positive mass spectrum, which also contains OC fragments such as $[C_3H]^+$ (m/z 37), $[C_2HO]^+$ (m/z 41), $[CH_3CO]^+$ (m/z 43), $[C_4H_3]^+$ (m/z 51), $[C_5H_3]^+$ (m/z 63), and $[C_6H_2]^+$ (m/z 74). In the negative mass spectrum, $[C_2H_2]^-$ (m/z −26), $[Cl]^-$ (m/z −35 and −37), $[NO_2]^-$ (m/z −46), $[C_2H_3O_2]^-$ (m/z −59), $[NO_3]^-$ (m/z −62), and $[C_6H]^-$ (m/z −73) are all present. The results of the controlled smoldering experiments indicate that this ECOC particle type probably originates from the smoldering of pine and cypress branches during meat smoking activities (see Section 3.3).

OC (1.0%). The positive mass spectrum contains aromatic ions such as $[C_3H_3]^+/K^+$ (m/z 39), $[C_4H_3]^+$ (m/z 51), m/z 63 $[C_6H_3)]^+$, $[C_6H_5]^+$ (m/z 77), and $[C_7H_7]^+$ (m/z 91) (Gross et al., 2000), while nitrate and sulfate dominate the negative mass spectrum.

ECOC-NH$_4$ (1.0%). The average mass spectrum of this particle type is similar to that of ECOC, but also contains the NH_4^+ ion (m/z 18). The presence of strong signals for other secondary inorganic species (sulfate and nitrate) indicates that ECOC-NH_4 particles are aged. In addition, ECOC-NH_4 is comparable to a BB particle type with an irregular shape, containing ammoniated sulfate, organic matter, and soot (Li et al., 2011b).

Fe-rich (1.5%). Iron (m/z 54 and 56) is dominant in the positive mass spectrum, which also contains carbon ($[C_n]^+$) and hydrocarbon fragments ($[C_xHy]^+$). Sulfate and nitrate dominate the negative mass spectrum. The Fe-rich particle type has a size distribution peaking around 0.8 μm and is likely due to a dust component. We have also reported a similar Fe type in Xi'an during wintertime (Chen et al., 2016). A Fe-rich cluster with the similar chemical composition was in an irregular shape (Li et al., 2017), and the chemical composition pattern suggests that it could be from coal burning (Silva et al., 2009).

ECOC-aged (3.0%). This particle type is similar in composition to ECOC but highly aged with strong sulfate and nitrate peaks and only minor ammonium uptake.

Pb-rich (1.0%). Pb is evident in the positive mass spectrum at m/z 206, 207 and 208, which also contains other metallic species including Cr (m/z 52), Cu (m/z 63 and 65) and Zn (m/z 64). The negative mass spectrum contains peaks due to $[Cl]^-$ (m/z −35 and −37), $[CNO]^-$ (m/z −42), PO_3^- (m/z −79), which along with the metallic content, points to a combustion source such as waste incineration (Chen et al., 2016; Moffet et al., 2008). The Pb-rich particle cluster could be spherical, elliptical, and chain-like; Pb is commonly in Pb oxides, but it could also be found in the form of $PbSO_4$ (Li et al., 2017).

Other (0.5%). Potassium dominates the positive mass spectrum of this particle type, which also contains a several hydrocarbon fragments ($[C_4H_7]^+$ at m/z 55 and $[C_5H_3]^+$ at m/z 63), as well as oxidized hydrocarbon ions ($[C_2H_3O]^+$ (m/z 43), indicative of secondary organic carbon.

NaK-dust (5.0%). The average mass spectrum contains sodium, potassium, nitrate, and sulfate and is similar to that reported for dust particles in other studies (Dall'osto and Harrison, 2006). The NaK-dust particle type had a size distribution centered around 0.75 μm in the accumulation mode, noticeably larger than the combustion particle types which peaked around 0.5 μm (Fig. S1). This NaK-dust particle type is also rich in ammonium and hydrocarbon fragments ($[C_3H]^+$ and $[C_2H_3O]^+$). The weak peak at m/z −60 suggests that the dust particle has a low mass fraction of carbonate $[CO_3]^{2-}$, which has possibly been displaced by sulfate and nitrate via heterogeneous reactions with acidic gasses like SO_2 and HNO_3 (Sullivan et al., 2009).

Overall, in the SPAMS dataset, the most abundant particle class was BB (33%), followed by KSec (29%), K-EC (20%), NaK-dust (5%), and ECOC (5%). The vast majority (>90%) of the particle types are carbonaceous in nature and attributed to biomass burning. With the exception of BB and ECOC, most of the particle types also showed appreciable signs of aging in the stagnant air conditions.

3.3. Controlled smoldering experiments

Smoldering experiments were performed using a combination of dry wood logs and the pine/cypress branches mainly produced BB particles, with only a small fraction (ca. 1%) attributed to ECOC types. Since BB particles could be produced from any general wood burning activities, they are not a specific marker for biomass burning emissions from meat smoking. Consequently, here we focus on results obtained from smoldering experiments performed using only the pine and cypress branches in order to identify more specific particle types from this source.

Fig. 4a shows the average mass spectrum of particles emitted from the smoldering of fresh pine branches, twigs, and needles. The spectrum is abundant in potassium (m/z 39 and 41), $[K_2Cl]^+$ (m/z 113 and 115), $[CN]^-$, $[CNO]^-$ (m/z −46 and −62), levoglucosan markers (−45, −59, and −71), and Polycyclic Aromatic Hydrocarbon (PAH) ion fragments (m/z > 150). Similar mass spectra are commonly observed for particles produced from fresh biomass combustion (Guazzotti et al., 2003; Moffet et al., 2008; Pagels et al., 2013; Silva et al., 1999). The ART-2a clustering procedure was conducted to interpret the data produced from the smoldering experiments (SE). Four main clusters were identified; BB_SE_Pine (47%), ECOC_SE_Pine (37%), and OC_SE_Pine (11%), and Other (5%). The mass spectra of the three identifiable particle types are shown in Fig. 4b–d. They are similar to the BB, ECOC and OC particle types observed in the field, but have significantly less uptake of sulfate and nitrate. This difference may be attributed to the rapid uptake of nitrate and sulfate by the ambient combustion particles under the highly polluted and stagnant conditions present in Chongqing. A similarly rapid processing of particles was also observed during stagnant air conditions in Xi'an (Chen et al., 2016). Lewis et al. (2009) reported the chemical composition and morphology of ponderosa pine combustion particles, suggests the particles were in an irregular shape and composed of organic materials with soot inclusions. These particles possibly resemble the ECOC types reported in this study.

A number of similar results were obtained for the smoldering of fresh cypress branches, twigs, and needles (Fig. 5). The average mass spectrum of the smoldering cypress particles shows many of the same features that are present in the pine mass spectrum, but with weaker signals for PAHs, $[CN]^-$, and $[CNO]^-$. Again, four main clusters were identified using ART-2a analysis, including BB_SE_-Cyp (52%), ECOC_SE_Cyp (35%), and OC_SE_Cyp (9%) and Other (4%). The mass spectra of these particle types (Fig. 5b–d) were virtually identical to those produced from smoldering of pine and also bear strong similarities to their equivalents observed in the

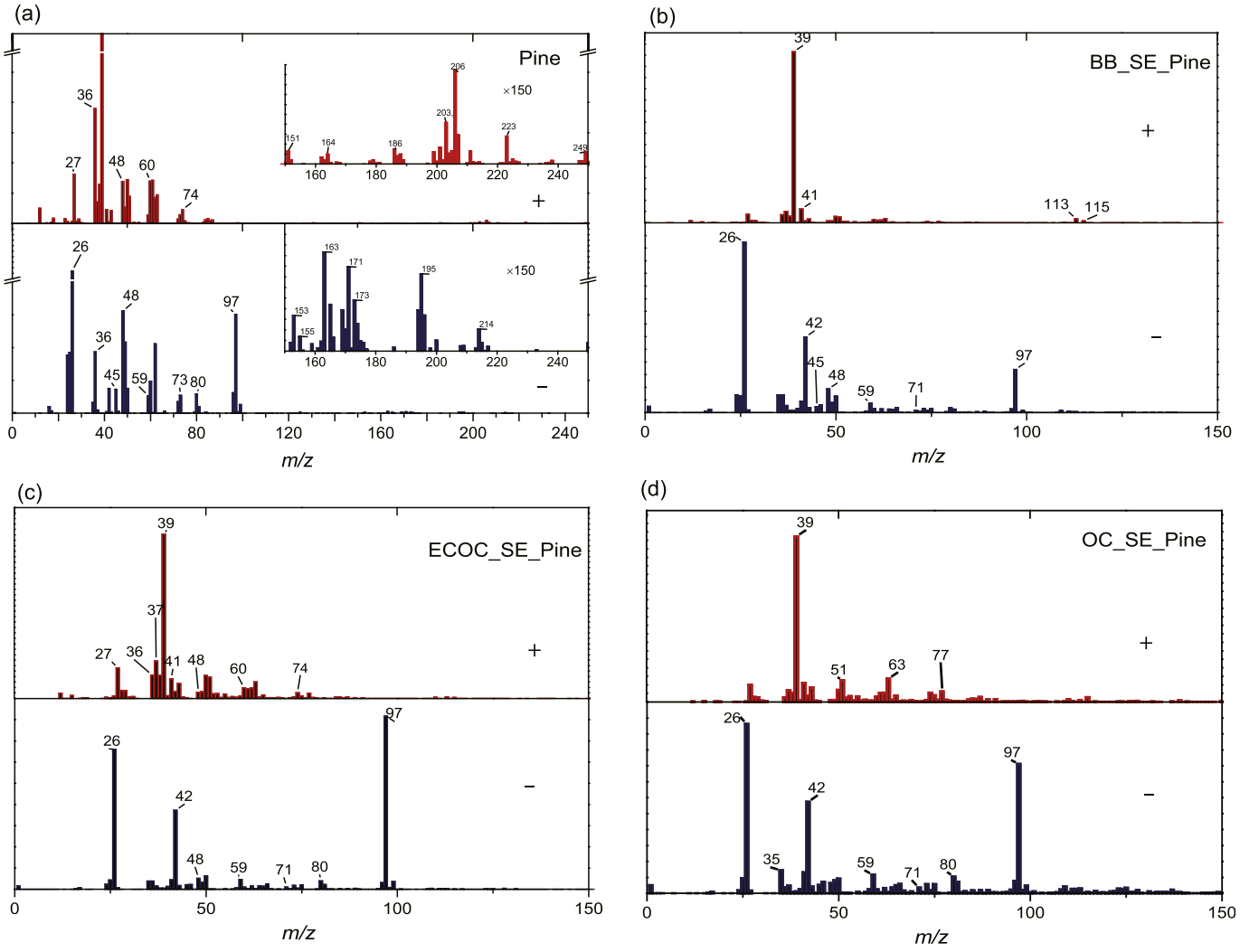

Fig. 4. SPAMS mass spectra of particles produced during the controlled smoldering of pine branches, twigs, and needles; (a) overall average mass spectrum; (b) ART-2a clustered BB particle type (BB_SE_Pine); (c) ART-2a clustered ECOC particle type (ECOC_SE_Pine), (d) ART-2a clustered OC particle type (OC_SE_Pine).

ambient air of Chongqing city, with the exception of nitrate uptake.

The most specific particle type attributable to the meat smoking activities in Chongqing is ECOC, whose mass spectrum is similar to ECOC_SE_Pine and ECOC_SE_Cyp. Indeed, there are good correlations between the field and smoldering mass spectra in the range $-150 < m/z < 150$, with the values of coefficient of determination (R^2) of 0.79 and 0.69 for pine and cypress, respectively. The main differences between the controlled smoldering particles and the ambient ECOC ones are that the latter contain smaller peaks for hydrocarbon fragments like $[C_2H_3]^+$ (m/z 27) and organonitrogen species $[CN]^-$ (m/z −26), and larger peaks for oxidized species like oxalic acid ($[COOCOOH]^-$ (m/z −89)) (Pratt et al., 2011). The uptake of secondary species such as ammonium, sulfate, and nitrate was also significantly more pronounced in the ambient ECOC particles.

Interestingly, the smoldering experiments did not produce particles with a chemical composition similar to that of K-EC, implying that K-EC is an aged particle type formed via atmospheric processing in the polluted air. Another possibility is that K-EC was a primary particle type produced from outdoor meat-smoking in Chongqing, but not in the controlled smoldering experiments. Combustion efficiency has been shown to affect the EC/OC ratio of particulate emissions and K-EC particle types are known to be more abundant at higher temperatures (Pagels et al., 2013). The absence of K-EC in the smoldering experiments could therefore be due to lower combustion temperatures than those performed during outdoor meat-smoking.

3.4. Temporal trends

The temporal trends of the various particle types are shown in terms of number fraction at 1 h time resolution in Fig. 2e. In Stage I, KSec and BB are major particle types, accounting for around 60–70% of the total particle population. At the onset of the pollution event on 12/26/2014, the total number of counts detected by the SPAMS increased dramatically, with the largest change in number fraction occurring for the K-EC particle type, whose contribution quickly grew from 2% (in Stage I) to over 20%. The K-EC number fraction gradually reduced during the pollution event until 01/05/2015 where another sharp increase occurred, raising it to 35%. The periods where K-EC peaked were characterized by extremely low wind speeds (0.5 m s^{-1}), indicating that these are locally emitted aged particles. As expected, the number fraction of fresh BB particles shows opposite behavior and peaks when K-EC was at its lowest. The introduction of the ban on biomass burning on 01/04/2015 resulted in a dramatic drop in BB number fraction as

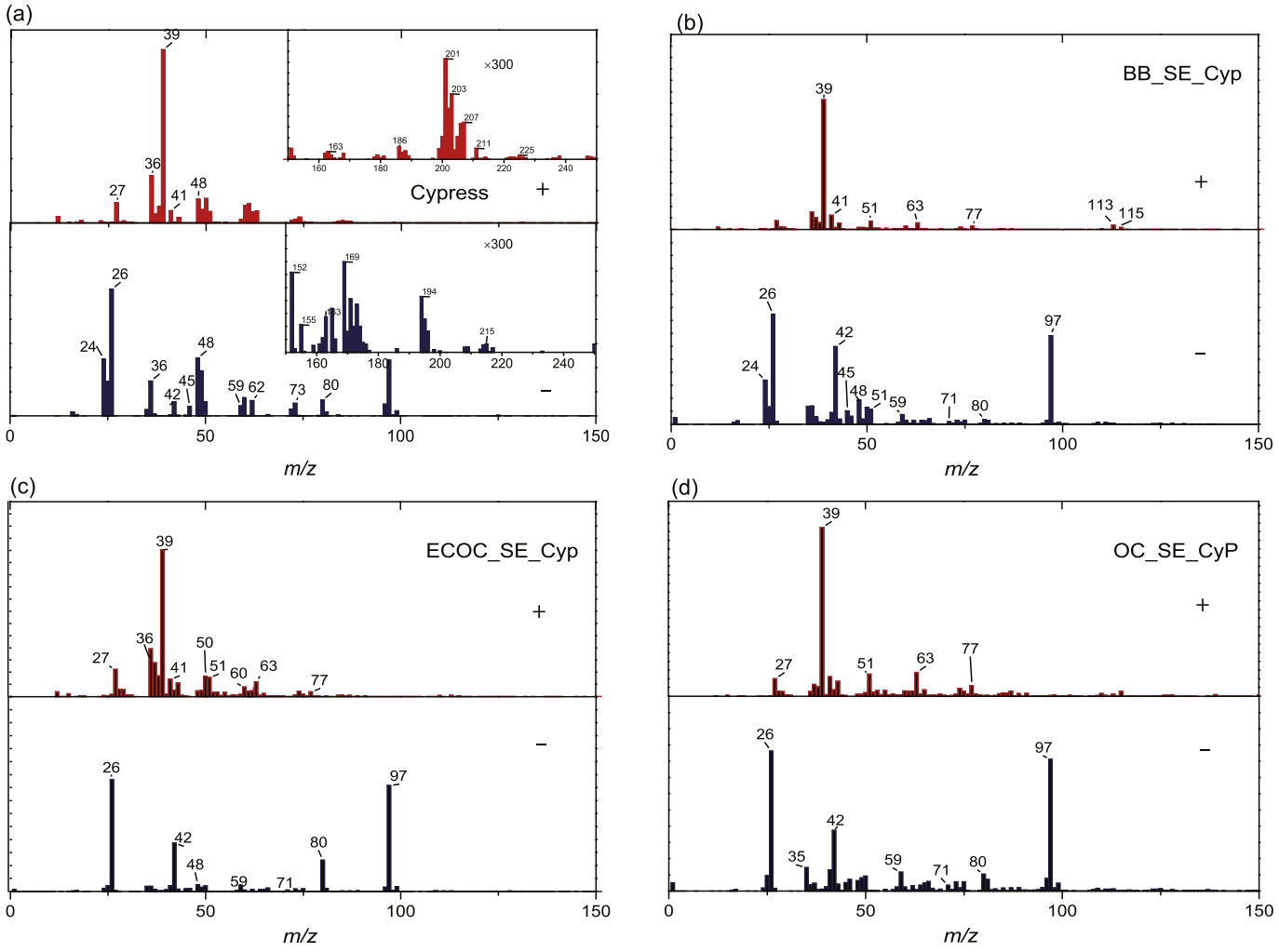

Fig. 5. SPAMS mass spectra of particles produced during the controlled smoldering of cypress branches, twigs and needles; (a) overall average mass spectrum; (b) ART-2a clustered BB particle type (BB_SE_Cyp); (c) ART-2a clustered ECOC particle type (ECOC_SE_Cyp), (d) ART-2a clustered OC particle type (OC_SE_Cyp).

residents and local restaurants burnt less wood. However, outdoor meat smoking activities did not stop completely as residents simply used more pine and cypress branches/twigs instead of the dry wood. This explains why there was a large increase in the ECOC number fraction even though the amount of BB decreased (Fig. 2e) during this period. Finally, in Stage III the total number of SPAMS counts dropped significantly as the particulate pollution is finally dispersed by winds. However, the total number fraction of fresh and aged biomass burning particles (BB, KSec, K-EC, ECOC, ECOC-aged) remained high.

3.5. Origins of particulate pollution

In Chongqing, the average consumption of pork per capita is 37.5 kg per year, with 2–5 kg of this amount attributed to preserved meat. The meat smoking process lasts for 12–48 h and typically consumes 20–40 kg biomass per 100 kg meat. Using these figures, it is estimated that somewhere in the region of 5–25 Gg of biomass is used to smoke meat in Chongqing city on an annual basis. Assuming that the number of particles emitted during smoldering was proportional to the biofuel mass, specifically, 10–30% of biofuel (e.g. pine and cypress) generated 10–30% of the total particle counts, meat smoking contributed at least 30% of all ambient BB particles (BB, KSec, ECOC, K-EC, etc.), and at most 90%. This estimate is of course subject to the limitations of the SPAMS instrument in relation to particle hit rates and transmission efficiency Li et al. (2011a). While mass scaling of the SPAMS data will likely produce a more certain estimate (Healy et al., 2012), it is still reasonable to assume that meat-smoking activities were a major source of particulate pollution during the observation period in Chongqing city.

Air mass trajectories and satellite fire maps were analyzed in order to rule out the possible contribution of agricultural burning or wildfires to the observed $PM_{2.5}$ levels in Chongqing city. The results, shown in Fig. 6 confirm that no fires were on the routes of the air masses passing Chongqing during the pollution event.

4. Conclusions

SPAMS was used for the first time to characterize a severe particulate pollution event in Chongqing city during the winter of 2014–2015. Biomass burning particles were predominant during the event, accounting for over 92.5% of the total number of counts in the SPAMS dataset. Outdoor meat smoking activities and stagnant weather conditions were the major contributing factors to the sustained period of $PM_{2.5}$ pollution. A series of experiments on the smoldering of locally sourced pine and cypress branches showed that an ECOC particle type was the most suitable marker for meat smoking activities, while all other biomass burning particles could

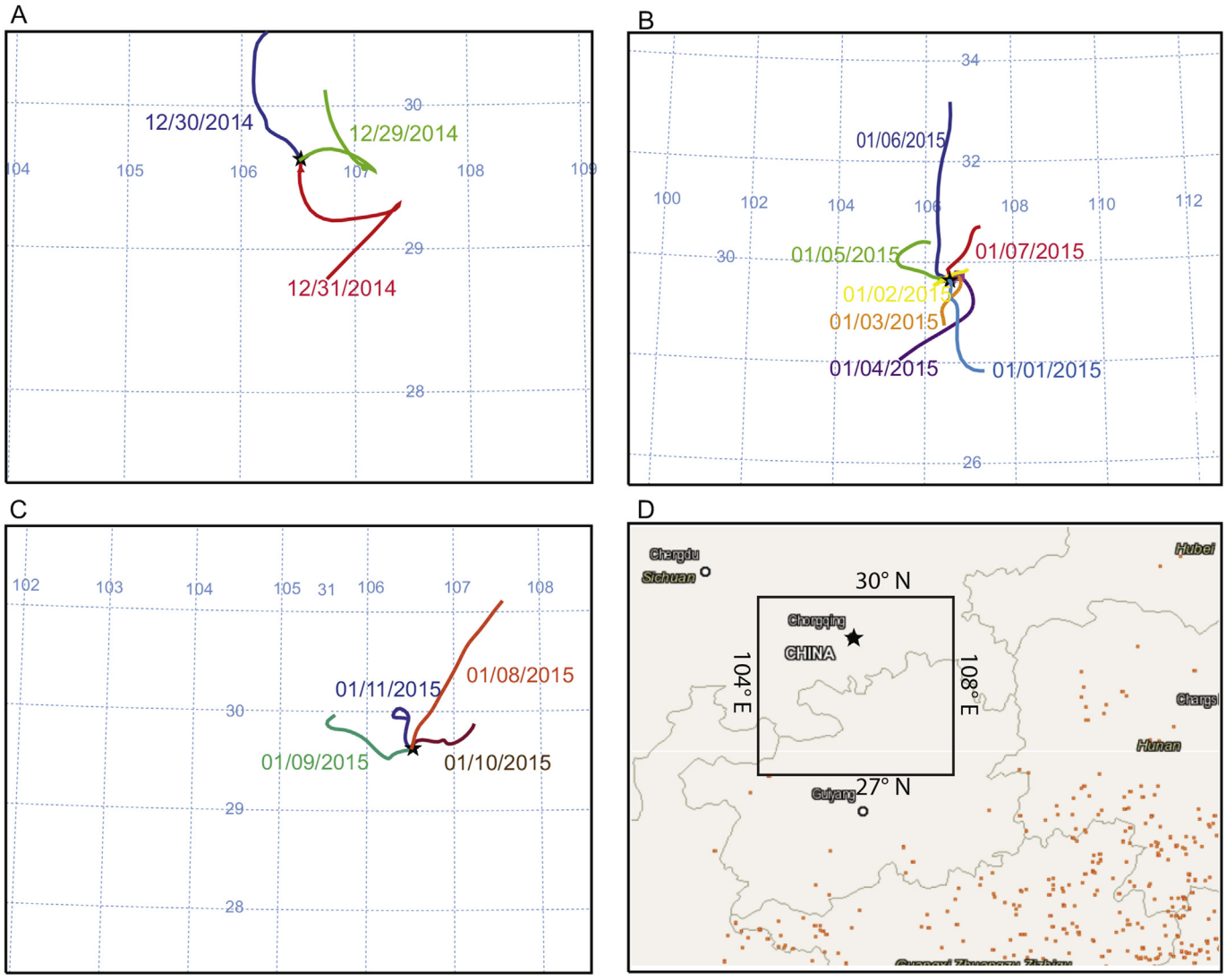

Fig. 6. Air masses arriving at Chongqing (denoted by a black star in each panel) with the height of 500 m above ground level for selected periods; (A) from 12/29/2014 to 12/31/2014 (B) from 01/01/2015 to 01/07/2015; (C) from 01/08/2015 to 01/11/2015.(D) The Firemap in China from 12/20/2014 to 01/10/2015 (data from https://firms.modaps.eosdis.nasa.gov/firemap/), where each brown dot represents a fire spot; the rectangle around Chongqing with longitude from 104°E to 108°E, latitude from 27°N to 30°N, covering the area of all the air mass backward trajectories displayed in Panels A, B, and C. (For interpretation of the references to colour in this figure legend, the reader is referred to the web version of this article.)

be attributed to more general forms of wood/biofuel combustion, e.g. in local restaurants and for home heating, as well as meat smoking. The introduction of a government ban on wood burning during the pollution event did reduce levels of local biomass burning emissions. However, many residents continued their outdoor meat smoking activities using more pine and cypress branches instead of wood. The traditional activity of making preserved meat in southwestern China is shown here to be a major source of local pollution and measures to reduce emissions should be introduced in order to improve air quality.

Acknowledgements

Financial support from Nature Science Foundation of China (Grant No. 41375123 and 41230641), "Strategic Priority Research Program" of the Chinese Academy of Sciences (Grant No. KJZD-EW-TZ-G06-04 and XDA05100401), Key Lab of Aerosol Physics and Chemistry, Chinese Academy of Sciences, and "Western Talents" of Chinese Academy of Sciences, and Chongqing Science and Technology Commission (Grant N0. cstc2015jcyjA20003, cstc2014yykfC20003, cstckjcxljrc13) are acknowledged. The authors are grateful for the assistance and information provided by staff in the Chongqing Environmental Monitoring Station.

Appendix A. Supplementary data

Supplementary data related to this article can be found at http://dx.doi.org/10.1016/j.envpol.2017.05.022.

References

Bi, X.H., Zhang, G.H., Li, L., Wang, X.M., Li, M., Sheng, G.Y., Fu, J.M., Zhou, Z., 2011. Mixing state of biomass burning particles by single particle aerosol mass spectrometer in the urban area of PRD, China. Atmos. Environ. 45, 3447–3453.
Cao, J., 2014. $PM_{2.5}$ and Environment in China. Science Press, Beijing.
Cao, J.J., Lee, S.C., Chow, J.C., Watson, J.G., Ho, K.F., Zhang, R.J., Jin, Z.D., Shen, Z.X., Chen, G.C., Kang, Y.M., Zou, S.C., Zhang, L.Z., Qi, S.H., Dai, M.H., Cheng, Y., Hu, K., 2007. Spatial and seasonal distributions of carbonaceous aerosols over China. J. Geophys. Res. 112, D22S11.
Chen, K., Yin, Y., Kong, S., Xiao, H., Wu, Y., Chen, J., Li, A., 2014. Size-resolved

chemical composition of atmospheric particles during a straw burning period at Mt. Huang (the Yellow Mountain) of China. Atmos. Environ. 84, 380–389.
Chen, Y., Cao, J., Huang, R., Yang, F., Wang, Q., Wang, Y., 2016. Characterization, mixing state, and evolution of urban single particles in Xi'an (China) during wintertime haze days. Sci. Total Environ. 573, 937–945.
Chen, Y., Yang, F., Mi, T., Cao, J., Shi, G., Huang, R., Wang, H., Chen, J., Lou, S., Wang, Q., 2017. Characterizing the composition and evolution of urban particles in Chongqing (China) during summertime. Atmos. Res. 187, 84–94.
Cheng, Z., Wang, S., Fu, X., Watson, J.G., Jiang, J., Fu, Q., Chen, C., Xu, B., Yu, J., Chow, J.C., Hao, J., 2014. Impact of biomass burning on haze pollution in the Yangtze River delta, China: a case study in summer 2011. Atmos. Chem. Phys. 14, 4573–4585.
Dall'osto, M., Harrison, R., 2006. Chemical characterisation of single airborne particles in Athens (Greece) by ATOFMS. Atmos. Environ. 40, 7614–7631.
Draxler, R.R., Hess, G.D., 1998. An overview of the HYSPLIT 4 modeling system for trajectories, dispersion and deposition. Aust. Meteorol. Mag. 47, 295.
Gross, D.S., Galli, M.E., Silva, P.J., Wood, S.H., Liu, D.Y., Prather, K.A., 2000. Single particle characterization of automobile and diesel truck emissions in the Caldecott Tunnel. Aerosol Sci. Technol. 32, 152–163.
Guazzotti, S.A., Suess, D.T., Coffee, K.R., Quinn, P.K., Bates, T.S., Wisthaler, A., Hansel, A., Ball, W.P., Dickerson, R.R., Neususs, C., Crutzen, P.J., Prather, K.A., 2003. Characterization of carbonaceous aerosols outflow from India and Arabia: biomass/biofuel burning and fossil fuel combustion. J. Geophys. Research-Atmospheres 108, 4485.
He, M., Zheng, J., Yin, S., Zhang, Y., 2011. Trends, temporal and spatial characteristics, and uncertainties in biomass burning emissions in the Pearl River Delta, China. Atmos. Environ. 45, 4051–4059.
Healy, R.M., Hellebust, S., Kourtchev, I., Allanic, A., O'Connor, I.P., Bell, J.M., Healy, D.A., Sodeau, J.R., Wenger, J.C., 2010. Source apportionment of $PM_{2.5}$ in Cork Harbour, Ireland using a combination of single particle mass spectrometry and quantitative semi-continuous measurements. Atmos. Chem. Phys. 10, 9593–9613.
Healy, R.M., Sciare, J., Poulain, L., Kamili, K., Merkel, M., Muller, T., Wiedensohler, A., Eckhardt, S., Stohl, A., Sarda-Esteve, R., McGillicuddy, E., O'Connor, I.P., Sodeau, J.R., Wenger, J.C., 2012. Sources and mixing state of size-resolved elemental carbon particles in a European megacity: Paris. Atmos. Chem. Phys. 12, 1681–1700.
Huang, R.J., Zhang, Y., Bozzetti, C., Ho, K.F., Cao, J.J., Han, Y., Daellenbach, K.R., Slowik, J.G., Platt, S.M., Canonaco, F., Zotter, P., Wolf, R., Pieber, S.M., Bruns, E.A., Crippa, M., Ciarelli, G., Piazzalunga, A., Schwikowski, M., Abbaszade, G., Schnelle-Kreis, J., Zimmermann, R., An, Z., Szidat, S., Baltensperger, U., El Haddad, I., Prevot, A.S., 2014. High secondary aerosol contribution to particulate pollution during haze events in China. Nature 514, 218–222.
Huang, Y., Li, L., Li, J., Wang, X., Chen, H., Chen, J., Yang, X., Gross, D.S., Wang, H., Qiao, L., Chen, C., 2013. A case study of the highly time-resolved evolution of aerosol chemical and optical properties in urban Shanghai, China. Atmos. Chem. Phys. 13, 3931–3944.
Jimenez, J.L., Canagaratna, M.R., Donahue, N.M., Prevot, A.S., Zhang, Q., Kroll, J.H., DeCarlo, P.F., Allan, J.D., Coe, H., Ng, N.L., Aiken, A.C., Docherty, K.S., Ulbrich, I.M., Grieshop, A.P., Robinson, A.L., Duplissy, J., Smith, J.D., Wilson, K.R., Lanz, V.A., Hueglin, C., Sun, Y.L., Tian, J., Laaksonen, A., Raatikainen, T., Rautiainen, J., Vaattovaara, P., Ehn, M., Kulmala, M., Tomlinson, J.M., Collins, D.R., Cubison, M.J., Dunlea, E.J., Huffman, J.A., Onasch, T.B., Alfarra, M.R., Williams, P.I., Bower, K., Kondo, Y., Schneider, J., Drewnick, F., Borrmann, S., Weimer, S., Demerjian, K., Salcedo, D., Cottrell, L., Griffin, R., Takami, A., Miyoshi, T., Hatakeyama, S., Shimono, A., Sun, J.Y., Zhang, Y.M., Dzepina, K., Kimmel, J.R., Sueper, D., Jayne, J.T., Herndon, S.C., Trimborn, A.M., Williams, L.R., Wood, E.C., Middlebrook, A.M., Kolb, C.E., Baltensperger, U., Worsnop, D.R., 2009. Evolution of organic aerosols in the atmosphere. Science 326, 1525–1529.
Lewis, K., Arnott, W.P., Moosmuller, H., Chakrabarty, R.K., Carrico, C.M., Kreidenweis, S.M., Day, D.E., Malm, W.C., Laskin, A., Jimenez, J.L., 2009. Reduction in biomass burning aerosol light absorption upon humidification: roles of inorganically-induced hygroscopicity, particle collapse, and photoacoustic heat and mass transfer. Atmos. Chem. Phys. 9, 8949–8966.
Li, L., Huang, Z.X., Dong, J.G., Li, M., Gao, W., Nian, H.Q., Fu, Z., Zhang, G.H., Bi, X.H., Cheng, P., Zhou, Z., 2011a. Real time bipolar time-of-flight mass spectrometer for analyzing single aerosol particles. Int. J. Mass Spectrom. 303, 118–124.
Li, L., Li, M., Huang, Z.X., Gao, W., Nian, H.Q., Fu, Z., Gao, J., Chai, F.H., Zhou, Z., 2014. Ambient particle characterization by single particle aerosol mass spectrometry in an urban area of Beijing. Atmos. Environ. 94, 323–331.
Li, R., Yang, X., Fu, H., Hu, Q., Zhang, L., Chen, J., 2017. Characterization of typical metal particles during haze episodes in Shanghai, China. Chemosphere 181, 259–269.
Li, W., Zhou, S., Wang, X., Xu, Z., Yuan, C., Yu, Y., Zhang, Q., Wang, W., 2011b. Integrated evaluation of aerosols from regional brown hazes over northern China in winter: concentrations, sources, transformation, and mixing states. J. Geophys. Res. 116.
Li, W.J., Shao, L.Y., Buseck, P.R., 2010. Haze types in Beijing and the influence of agricultural biomass burning. Atmos. Chem. Phys. 10, 8119–8130.
Moffet, R.C., de Foy, B., Molina, L.T., Molina, M.J., Prather, K.A., 2008. Measurement of ambient aerosols in northern Mexico City by single particle mass spectrometry. Atmos. Chem. Phys. 8, 4499–4516.
Onasch, T.B., Trimborn, a., Fortner, E.C., Jayne, J.T., Kok, G.L., Williams, L.R., Davidovits, P., Worsnop, D.R., 2012. Soot particle aerosol mass spectrometer: development, validation, and initial application. Aerosol Sci. Technol. 46, 804–817.
Pagels, J., Dutcher, D.D., Stolzenburg, M.R., McMurry, P.H., Galli, M.E., Gross, D.S., 2013. Fine-particle emissions from solid biofuel combustion studied with single-particle mass spectrometry: identification of markers for organics, soot, and ash components. J. Geophys. Research-Atmospheres 118, 859–870.
Pratt, K.A., Heymsfield, A.J., Twohy, C.H., Murphy, S.M., DeMott, P.J., Hudson, J.G., Subramanian, R., Wang, Z., Seinfeld, J.H., Prather, K.a, 2010. Situ chemical characterization of aged biomass-burning aerosols impacting cold wave clouds. J. Atmos. Sci. 67, 2451–2468.
Pratt, K.A., Murphy, S.M., Subramanian, R., DeMott, P.J., Kok, G.L., Campos, T., Rogers, D.C., Prenni, A.J., Heymsfield, A.J., Seinfeld, J.H., Prather, K.A., 2011. Flight-based chemical characterization of biomass burning aerosols within two prescribed burn smoke plumes. Atmos. Chem. Phys. 11, 12549–12565.
Pratt, K.A., Prather, K.A., 2012. Mass spectrometry of atmospheric aerosols—recent developments and applications. Part II: on-line mass spectrometry techniques. Mass Spectrom. Rev. 31, 17–48.
Qin, X.Y., Pratt, K.A., Shields, L.G., Toner, S.M., Prather, K.A., 2012. Seasonal comparisons of single-particle chemical mixing state in Riverside, CA. Atmos. Environ. 59, 587–596.
Reid, J.S., Koppmann, R., Eck, T.F., Eleuterio, D.P., 2005. A review of biomass burning emissions part II: intensive physical properties of biomass burning particles. Atmos. Chem. Phys. 5, 799–825.
Robinson, A.L., Donahue, N.M., Shrivastava, M.K., Weitkamp, E.A., Sage, A.M., Grieshop, A.P., Lane, T.E., Pierce, J.R., Pandis, S.N., 2007. Rethinking organic aerosols: semivolatile emissions and photochemical aging. Science 315, 1259–1262.
Silva, L.F.O., Moreno, T., Querol, X., 2009. An introductory TEM study of Fe-nanominerals within coal fly ash. Sci. Total Environ. 407, 4972–4974.
Silva, P.J., Liu, D.-Y., Noble, C.A., Prather, K.A., 1999. Size and chemical characterization of individual particles resulting from biomass burning of local southern California species. Environ. Sci. Technol. 33, 3068–3076.
Simoneit, B.R.T., 2002. Biomass burning — a review of organic tracers for smoke from incomplete combustion. Appl. Geochem. 17, 129–162.
Song, X.H., Hopke, P.K., Fergenson, D.P., Prather, K.A., 1999. Classification of single particles analyzed by ATOFMS using an artificial neural network, ART-2A. Anal. Chem. 71, 860–865.
Sullivan, R.C., Moore, M.J.K., Petters, M.D., Kreidenweis, S.M., Roberts, G.C., Prather, K.A., 2009. Effect of chemical mixing state on the hygroscopicity and cloud nucleation properties of calcium mineral dust particles. Atmos. Chem. Phys. 9, 3303–3316.
Wang, H., Zhu, B., Zhang, Z., An, J., Shen, L., 2015. Mixing state of individual carbonaceous particles during a severe haze episode in January 2013, Nanjing, China. Particuology 20, 16–23.
Wang, J., Ge, X., Chen, Y., Shen, Y., Zhang, Q., Sun, Y., Xu, J., Ge, S., Yu, H., Chen, M., 2016. Highly time-resolved urban aerosol characteristics during springtime in Yangtze River Delta, China: insights from soot particle aerosol mass spectrometry. Atmos. Chem. Phys. 16, 9109–9127.
Yang, F., Chen, H., Du, J., Yang, X., Gao, S., Chen, J., Geng, F., 2012. Evolution of the mixing state of fine aerosols during haze events in Shanghai. Atmos. Res. 104–105, 193–201.
Yang, F., Tan, J., Zhao, Q., Du, Z., He, K., Ma, Y., Duan, F., Chen, G., Zhao, Q., 2011. Characteristics of PM2.5 speciation in representative megacities and across China. Atmos. Chem. Phys. 11, 5207–5219.
Zauscher, M.D., Wang, Y., Moore, M.J., Gaston, C.J., Prather, K.A., 2013. Air quality impact and physicochemical aging of biomass burning aerosols during the 2007 San Diego wildfires. Environ. Sci. Technol. 47, 7633–7643.
Zhang, G., Han, B., Bi, X., Dai, S., Huang, W., Chen, D., Wang, X., Sheng, G., Fu, J., Zhou, Z., 2015. Characteristics of individual particles in the atmosphere of Guangzhou by single particle mass spectrometry. Atmos. Res. 153, 286–295.
Zhang, Y.-L., Cao, F., 2015. Is it time to tackle PM2.5 air pollutions in China from biomass-burning emissions? Environ. Pollut. 202, 217–219.